

# Beam tilt and angular dispersion in broad-bandwidth, nanosecond optical parametric oscillators

W. J. Alford, Russell J. Gehr, R. L. Schmitt, and A. V. Smith

Department 1128 Lasers, Optics and Remote Sensing, Sandia National Laboratories, Albuquerque, New Mexico 87185-1423

Gunnar Arisholm

Forsvarets Forskningsinstitutt (Norwegian Defence Research Establishment), P.O. Box 25, N-2007, Kjeller, Norway

Received January 22, 1999; revised manuscript received April 15, 1999

We show that the signal and idler beams generated by certain types of unseeded, nanosecond optical parametric oscillators are tilted and angularly dispersed and have anomalously large bandwidths. This effect is demonstrated in both laboratory measurements and a numerical model. We show how the optical cavity design influences the tilts and how these tilts can be eliminated or minimized. We also determine the conditions necessary for injection seeding of these parametric oscillators. © 1999 Optical Society of America

[S0740-3224(99)02409-1]

OCIS codes: 190.4970, 190.4410, 190.2620.

## 1. INTRODUCTION

Critically phase-matched parametric mixing in nonlinear crystals achieves phase matching by counteracting refractive-index dispersion with crystal birefringence. It always involves both extraordinary (*e*) and ordinary (*o*) polarizations. As is well known, *e*-polarized waves undergo birefringent walk-off, meaning that their Poynting vectors are tilted relative to their propagation vectors by a walk-off angle  $\rho$ . These tilts break the reflection symmetry in the walk-off plane, permitting the development of beam tilts in the mixing process.<sup>1</sup> This admits of the possibility that the beams generated in a critically phase-matched optical parametric oscillator (OPO) might be tilted relative to the axis of the optical cavity. A number of variables, such as the optical cavity design, the pump beam diameter, the walk-off angles, whether the resonated wave is an *e* or an *o* wave, and the degree of phase mismatch, might be expected to influence such tilts. Another well-known feature of critically phase-matched nonlinear mixing is that the phase-matching angle depends on the wavelengths. This dependence could lead to angular dispersion of the signal and idler wavelengths generated in a broad-bandwidth, critically phase matched OPO. For example, if a monochromatic pump wave is aligned along the cavity axis of a standing wave, type II (signal and idler orthogonally polarized) OPO, only one signal frequency will phase match along this axis. If the signal frequency deviates slightly from this value, the phase-matching angle shifts slightly, perhaps leading to angular dispersion of the output wavelengths. The degree of dispersion will depend primarily on the phase-matching properties of the crystal but most likely will also be influenced by the same design parameters as the tilt.

Signal beam tilts have been reported by Haub *et al.*<sup>2</sup> for a type II KTiOPO<sub>4</sub> (KTP) OPO, and dispersion has been noted in nominally collinear<sup>3</sup> and noncollinear<sup>4</sup> type I  $\beta$  BaB<sub>2</sub>O<sub>4</sub> OPO's and in a collinear-type II  $\beta$  BaB<sub>2</sub>O<sub>4</sub> OPO.<sup>4</sup> In this paper we report observation of tilts and dispersion both in laboratory measurements of a broad-bandwidth, critically phase-matched, standing-wave KTP OPO and in a numerical model of it, with good agreement between them. We explain in some detail based on an understanding gleaned from numerous computer simulations how tilts and dispersion develop, and we discuss ways to eliminate or minimize them. We also examine the requirements for injection seeding OPO's in their presence. Where possible we support our model-derived conclusions with laboratory observations.

## 2. NUMERICAL OPO MODEL

Our numerical model for broad-bandwidth, nanosecond OPO's accounts for nonlinear mixing, diffraction, birefringent walk-off, group velocity, and group-velocity dispersion of each wave. It also incorporates a realistic model of quantum noise, including multiple transverse and longitudinal modes, permitting us to model unseeded or free-running OPO's. The model numerically integrates three wave equations of the form<sup>5</sup>

$$\left( \frac{\partial}{\partial z} - \frac{i}{2k_j} \nabla_t^2 + \tan \rho_j \frac{\partial}{\partial x} + \frac{1}{v_j} \frac{\partial}{\partial t} + i\alpha_j \frac{\partial^2}{\partial t^2} \right) \epsilon_j(x, y, z, t) = P_j(x, y, z, t) \exp(\pm i\Delta kz), \quad (1)$$

where the subscript *j* refers to the signal, the idler, or the pump wave, the  $\nabla_t^2$  term accounts for diffraction, the  $\tan \rho_j$  term describes birefringent walk-off with angle  $\rho_j$  in

the  $x$  direction, the  $v_j$  and  $\alpha_j$  terms describe group velocity and group-velocity dispersion, respectively, and the  $P_j$  term is the driving polarization at frequency  $j$  that is due to second-order nonlinearity. We ignore linear absorption, nonlinear contributions to the refractive index, and multiphoton absorption. The phase mismatch  $\Delta k$  is defined as  $(k_p - k_s - k_i)$ ; the plus in the exponential of Eq. (1) applies to the signal and idler equations, whereas the minus applies for the pump equation. We use the split-step integration method in which linear propagation and nonlinear mixing are handled in alternating steps.<sup>6-9</sup> For the propagation half-step over distance  $\Delta z$ , we Fourier transform the fields  $\epsilon_j$  from  $\{x, y, z, t\}$  space to  $\{k_x, k_y, z, \omega\}$  space, shift the phase of each Fourier component as appropriate to account for diffraction, birefringent walk-off, group velocity, and group-velocity dispersion, and then Fourier transform back to  $\{x, y, z, t\}$  space. We then calculate the influence of the polarization term on  $\epsilon_j$  over the same  $\Delta z$  step. Quantum noise at the signal and idler frequencies is incident upon both mirrors from outside the cavity. This noise has a spectrum broader than the crystal's acceptance bandwidth and is spatially structured to include more transverse modes than are supported by the OPO. In the cases described here, group-velocity dispersion, nonlinear refractive index, and two-photon absorption are expected to be unimportant and are not included. Typical execution times are a few hours on a 300-MHz Pentium II computer. To shorten execution time and reduce memory demands, we sometimes follow the development of only a fraction of a round-trip time slice as it circulates in the cavity.<sup>7,9</sup> This approximation will obviously not model all aspects of the OPO perfectly, but we find that it gives a good approximation to the aspects of interest in this paper, namely, conversion efficiency, pump thresholds, spectral widths, beam tilts, and angular dispersion.

Using this model, we look first at the development of tilts. To focus on tilts without the added complexity of dispersion, we modeled monochromatic operation by limiting the injected noise to a single frequency while retaining its transverse spatial noise. The modeled device is the standing-wave OPO diagrammed in Fig. 1. It is pumped by a 10-ns, 532-nm pulse and contains a KTP nonlinear crystal oriented for operation at signal and idler wavelengths of 784 and 1655 nm, respectively. The pump and the idler are  $o$  polarized, and only the  $e$ -polarized signal wave is resonated. Birefringent signal walk-off in the 10-mm-long crystal is 0.487 mm, comparable with the pump beam diameter of 0.65 mm (FWHM). The physical cavity length is 12 mm. We begin with the KTP crystal aligned for exact phase matching with all beams parallel to the cavity axis. Throughout this discussion we define the phase mismatch  $\Delta k$  as that associated with this collinear geometry. With the mirror reflectivities set to zero for all waves, we first look at single-pass behavior and find that the amplified signal and idler beams exiting the crystal are tilted by a few microradians, with the signal bent in the direction opposite walk-off and the idler bent toward walk-off. This we attribute to gain guiding, a reflection of the fact that parametric gain is highest for signal light that best maintains spatial overlap with the pump and idler beams. When the mir-

ror signal reflectivities are set to 1.0 and 0.71, this gain-induced tilt causes the signal light initially to follow the course diagrammed in Fig. 2(a). Over many cavity round trips the signal beam moves to the antiwalk-off side of the pump beam and stabilizes there. At threshold, loosely defined as the point where the pump is significantly depleted, we find that at the crystal exit face both the signal and the idler beams are offset to the antiwalk-off side of the pump beam by approximately half of the pump diameter. This initial offset of the signal beam suggests that a small tilt of the crystal might tilt the phase-matching direction toward walk-off ( $\Delta k < 0$ ), and this might counteract the gain-induced tilt, reducing the signal offset and giving better beam overlap. We tried a range of values of  $\Delta k$  (or equivalently crystal tilts) with multitransverse

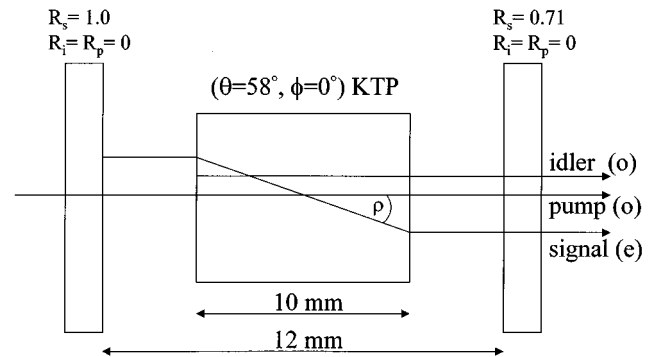


Fig. 1. The test OPO uses a 10-mm-long, type II phase-matched KTP crystal pumped by a 10-ns (FWHM), 532-nm, 0.65-mm-diameter (FWHM irradiance), single-longitudinal-mode pulse. The physical cavity length is 12 mm. The signal walk-off angle is 48.7 mrad;  $d_{\text{off}}$  is 3.0 pm/V; signal, idler, and pump refractive indices are 1.816, 1.735, and 1.790, respectively; signal, idler, and pump group-velocity indices are 1.876, 1.765, and 1.911, respectively; the phase-matching angle is  $\theta = 57^\circ$ ,  $\phi = 0^\circ$ .

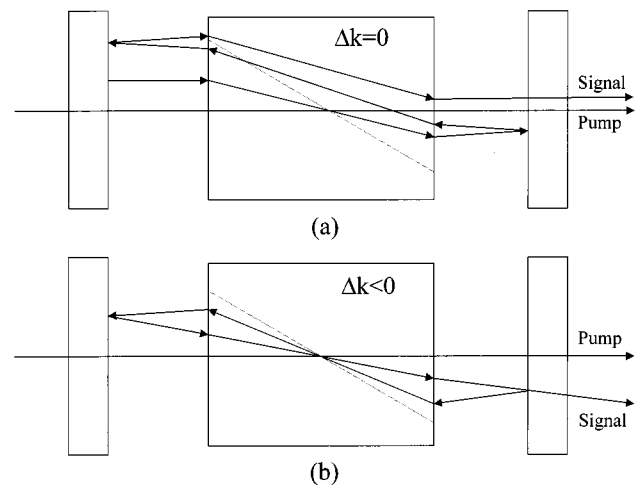


Fig. 2. (a) Beam path assumed by the signal wave in the monochromatic, phase-matched OPO, (b) signal beam path for the highest gain mode of operation. Dotted lines, the walk-off path for an  $e$ -polarized beam with its propagation vector along the cavity axis.  $\Delta k$ , collinear phase mismatch. Note that the tilt angles are greatly exaggerated; the actual beam tilts of  $\sim 5$  mrad are much smaller than the walk-off angle of  $\sim 50$  mrad.

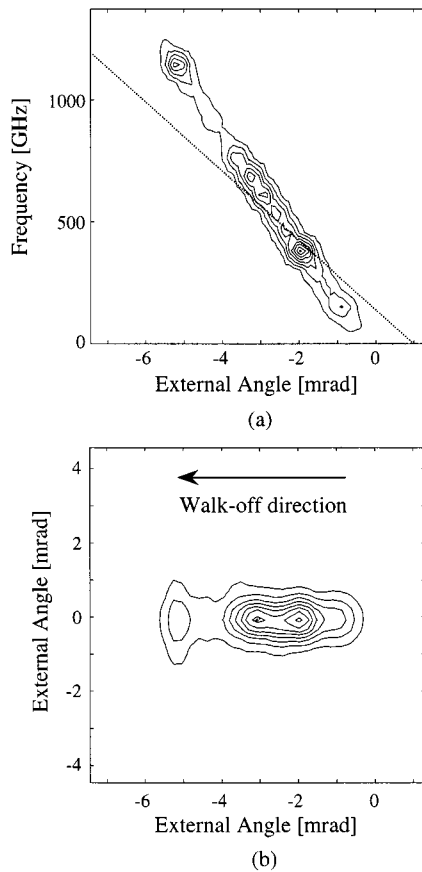


Fig. 3. (a) Model-generated contour plots of signal fluence for the test OPO versus angle relative to the cavity axis on the horizontal axis and detuning from the phase-matched wavelength on the vertical axis. Dotted line, the calculated phase-matching frequency versus crystal angle. (b) Far-field signal fluence contours.

mode (but still monochromatic) injected signal light and found that gain and conversion efficiency were maximum for negative values  $\Delta k$ . Gain was nearly constant over the range  $-19 < \Delta kL < -9.5$ , corresponding to tilts of the generated signal beam outside the OPO ranging from 2.3 to 4.5 mrad in the walk-off direction. This means that a monochromatic beam experiences the highest gain and earliest threshold not when the signal beam is aligned with the cavity axis and the crystal is phase matched for the signal beam along this axis but when the crystal is tilted slightly in the walk-off direction. The path followed by the signal beam then is diagrammed in Fig. 2(b). In these simulations we notice that, even with the crystal tilted for highest gain, the initial pump depletion is still displaced to the antiwalk-off side but by a smaller amount than before. As the pump power and gain diminish late in the pulse, gain guiding decreases, and we find that the zone of pump depletion gradually moves to the walk-off side, as would be expected for a signal beam with its propagation vector tilted in that direction. We note that the signal tilt is relatively constant during the signal pulse, having reached an equilibrium value during buildup to threshold, and the idler tilts in the direction opposite the signal at an angle larger by approximately  $(n_s \omega_s / n_i \omega_i)$ , as expected for transverse phase matching.

We deduce from this monochromatic modeling exercise that a given cavity design can have maximal gain at a nonzero phase mismatch. For different signal wavelengths this optimum value of  $\Delta k$  will occur at slightly different signal angles, of course, so for broad-bandwidth operation we might expect the signal wavelengths to be angle dispersed. In our OPO the bluer light will phase match better at larger tilts than the red light, so dispersion is such that the blue is tilted further in the walk-off direction than the red. We find that this is indeed the case when we initiate the model OPO with broad-bandwidth noise rather than with monochromatic noise, again keeping multiple transverse modes. Figure 3 shows results of such a simulation of our test OPO pumped at twice threshold (6 mJ), illustrating both tilt and angular dispersion. Figure 3(a) shows contours of signal fluence with beam tilt displayed on the horizontal axis and offset from the phase-matched frequency displayed on the vertical axis. Figure 3(b) shows the corresponding far-field fluence contours. The point (0, 0) in Fig. 3(a) corresponds to zero tilt relative to the cavity axis and to zero tuning from the frequency that is phase matched along the cavity axis. For our KTP crystal the variation of phase-matching angle with signal frequency is calculated from the Sellmeier equation<sup>10</sup> to be 3.41  $\mu\text{rad}/\text{GHz}$  internal to the crystal or 6.19  $\mu\text{rad}/\text{GHz}$  external, assuming near-normal incidence on the exit face. This is the dotted line in Fig. 3(a). The actual modeled dispersion is close to this value, but it is weakly influenced by cavity geometry, leading to a smaller value of  $\sim 5.4 \mu\text{rad}/\text{GHz}$ .

### 3. EXPERIMENT

Our experimental setup is shown in Fig. 4. The 532 nm pump light is provided by frequency-doubled output of a Q-switched, injection-seeded Nd:YAG laser in 10-ns, 12-mJ pulses. A variable attenuator and a spatial filter-telescope condition the pump light before the OPO. The filter-telescope uses a 500-mm focusing lens, a 275- $\mu\text{m}$ -diameter pinhole, and a 200-mm collimating lens to create a near-Gaussian spatial profile beam of diameter 0.65 mm (FWHM), corresponding to a maximum fluence at the OPO of 2.5  $\text{J}/\text{cm}^2$ . The 784-nm OPO seed light comes from a cw Ti:sapphire laser and has a maximum power of 20 mW. This beam is also spatially filtered and collimated to a diameter of 0.9 mm (FWHM). Both the pump and the seed beams are incident upon the OPO input mirror with reflectivities of 0.97 at 784 nm, 0.02 at 532 nm, and 0.18 at 1655 nm. The output coupler reflectivities are 0.72 at 784 nm, 0.008 at 532 nm, and 0.01 at 1655 nm. The input and output mirrors are flat. Our experimental procedure is to align the pump and seed beams carefully for collinear propagation and, with no mirrors installed, to adjust the crystal angle for maximum single-pass gain of the seed. This ensures that the crystal is aligned for zero phase mismatch in the direction of the beams. The OPO mirrors are then installed and adjusted to retro-reflect the seed and pump and to resonate the seed light with maximum finesse. We ramp the OPO cavity length by driving the piezoelectric transducer-mounted input mirror with a sawtooth voltage while adjusting the tilt of

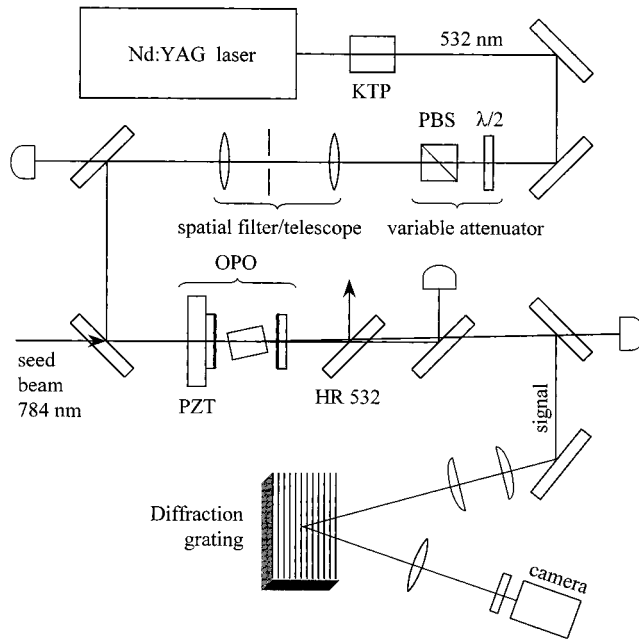


Fig. 4. Laboratory apparatus for characterizing KTP OPO's. Details are given in the text. PBS, polarizing beam splitter; PZT, piezoelectric transducer.

the output mirror to maximize contrast of the cavity transmission resonance fringes. Cavity length is then locked to a transmission peak by small-amplitude dithering of the cavity length with a lock-in stabilizer (Lansing 80.215). This procedure permits alignment with a precision of  $\sim 0.02$  mrad. According to the numerical model, a tilt of this magnitude should change the signal beam tilt by  $\sim 0.5$  mrad. We tested our alignment precision by repeatedly realigning the cavity and found that the signal tilt varied by less than 0.5 mrad among alignments. We conclude that our measurements have a tilt uncertainty of  $\sim 0.5$  mrad owing to cavity mirror misalignment. The model is capable of handling mirror tilts of at least 0.1 mrad, but we did not systematically study OPO performance with such large misalignments either experimentally or numerically.

We characterize the OPO signal pulse by several measurements. To determine the angle between the signal and the pump beams we propagate the beams 2 m beyond the OPO and measure the maximum and minimum distances between the signal beam (which, for unseeded operation, spreads out considerably) and the pump spot. The median value is used as the signal beam angle. We measure the conversion efficiency of the OPO by splitting off calibrated portions of the pump and signal beams for measurement by pyroelectric pulse energy meters (Laser Precision Rj-7200 Energy Ratiometers with RjP-735 heads). Their calibration is checked by comparison with calibrated laser calorimeters. Finally, for the measurement of signal beam angle versus wavelength (for unseeded operation) the signal beam is collimated in the direction orthogonal to walk-off ( $y$  direction) by two cylindrical lenses and impinges upon an 1800-line/mm grating to disperse the wavelengths in the  $y$  direction. A 250-mm focal-length lens focuses the negative first-order diffracted beam onto a video camera positioned 250 mm

away, so beam tilt angle and wavelength correspond to image positions displaced along the  $x$  and  $y$  axes, respectively. Far-field images of the signal beam are acquired by use of the same arrangement but with the cylindrical collimating lenses removed and with the grating replaced by a flat mirror.

#### 4. DISCUSSION

Representative dispersed and far-field energy flux contour images are shown in Fig. 5 for the same pump level as in Fig. 3 (6 mJ). Unlike the model results, these two profiles are for different pulses. Once again, the zero of the horizontal axis corresponds to the direction of the seed beam and the cavity axis, whereas the zero of the vertical axis corresponds to the frequency of the seed light. Note the absence of light at the seed frequency, a point that we discuss below. The measured dispersion of  $\sim 5.3$   $\mu\text{rad}/\text{GHz}$  is in good agreement with the model's value of 5.4  $\mu\text{rad}/\text{GHz}$ . Note that the measured linewidth is also in fair agreement with the model predictions.

Given the good agreement between model and experiment, we feel justified in applying the model to other OPO designs to draw useful conclusions about the behavior of various types of OPO and in particular to find ways to prevent tilts and dispersion. The most obvious peculiari-

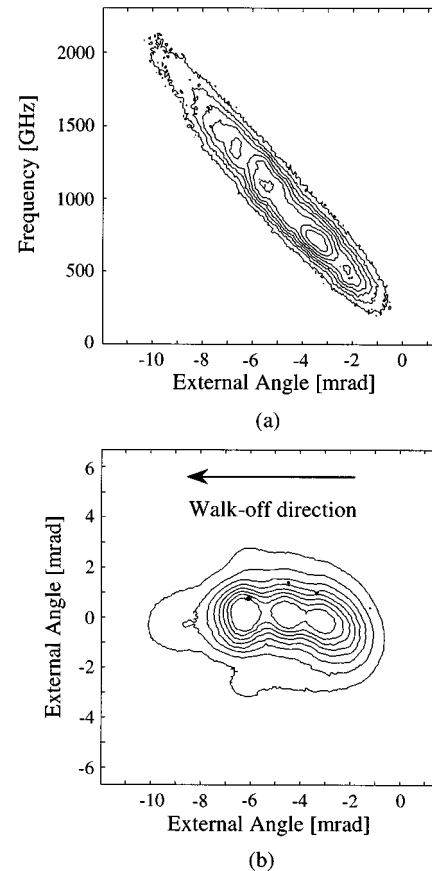


Fig. 5. (a) Measured contour plots of signal fluence for the test OPO versus angle relative to the cavity axis on the horizontal axis and detuning from the phase-matched wavelength on the vertical axis. (b) Far-field signal fluence contours.

ties of our OPO are the broad bandwidths and frequency shifts of signal and idler, along with their large tilts and angular spreads. Furthermore, we find that for higher pump energies, both angular and frequency spreads increase but the  $5.3 \mu\text{rad}/\text{GHz}$  dispersion is constant. The measured bandwidth of 1000–2000 GHz is much greater than the OPO acceptance bandwidth (defined as the signal frequency detuning for which  $\Delta kL = 2\pi$ ) of 270 GHz. Our type II OPO behaves quite differently from type I OPO's, which usually have bandwidths 2–5 times smaller than the acceptance bandwidth.<sup>3</sup>

Based on our understanding of the evolution of tilt and dispersion gleaned from the monochromatic model, we might anticipate that they could be avoided by use of multiple walk-off-compensating crystals in place of our single crystal. Gain guiding would tend to favor opposite tilts in the alternating crystals, nulling the net tilt. Alternatively, we could use a single crystal in a ring cavity that reversed the tilt on alternate passes, such as the three-mirror ring that was characterized in an earlier publication.<sup>8</sup> The plane of the ring lies in the walk-off plane, so a tilt induced on one pass assumes the opposite sign on the next. Our model indicates that these designs do indeed avoid tilt and dispersion almost entirely.

Table 1 summarizes model results for standing-wave and ring designs. The configurations labeled WOC-SW and Ring in Table 1 refer to the usual standing wave cavity with two walk-off-compensating crystals and to a single crystal in a three-mirror ring cavity with the same round-trip length, respectively. Both the walk-off-compensating and the ring designs eliminate tilts and dispersion and also narrow the linewidth, as we have verified by using the same KTP crystal in a ring cavity and using two walk-off-compensating 5-mm-long KTP crystals in place of the 10-mm-long KTP crystal in the usual standing-wave cavity. The observed tilts are less than our measurement uncertainty of 0.5 mrad in both cases. Both model and experiment also indicate that double passing the pump beam in our standing-wave design nearly eliminates signal and idler tilts. In this case, gain guiding on the return pass induces tilts opposite those created on the forward pass, at least during the buildup to threshold. Additionally, the optimal value of phase mismatch is zero, so there is no wavelength shift in these designs.

The configuration labeled SW in Table 1 refers to our usual standing-wave OPO but with walk-off and cavity resonance assigned to different beams. Apart from being assigned to different waves, the walk-off angles and mirror reflectivities are kept constant. From the listed results, we conclude that it matters little whether the resonated beam is the beam with walk-off. If either the signal or the idler has walk-off, there are tilts and detunings. However, the tilt of the resonated wave is nearly constant, whereas the other wave has a tilt to preserve transverse phase matching, so resonating the redder wave results in smaller tilts and detunings. Tilt directions are such that the *e*-polarized beam tilts in the direction of walk-off. For the standing-wave, single-pump-pass design with no walk-offs on any beam (noncritical phase matching), there is no tilt or dispersion, and the linewidth of the signal and the idler is substantially reduced. If walk-off is assigned to the pump rather than to the signal or the idler, as is appropriate for type I ( $e \leftarrow oo$ ) phase matching, there are no tilts, and the linewidth is approximately one quarter of the crystal's acceptance bandwidth, as expected. The same is true for type I ( $o \leftarrow ee$ ) phase matching.

If the beam path diagrammed in Fig. 2(b) is a valid explanation of signal tilts, lengthening the cavity while keeping crystal length constant should yield smaller tilts. We tested this hypothesis in the laboratory by using a variety of cavity lengths and found that, as expected, tilts diminish with increasing cavity length. Our results are summarized in Table 2. Not surprisingly, we also found that the threshold pump energy increases with cavity length because of delayed turn-on. The variation of tilt with pump diameter is more difficult to anticipate because gain guiding is influenced both by pump diameter and by the size of the signal-and-idler spatial structure. The model indicates that there is a slight increase in tilt and far-field angular spread with increasing pump diameter, but this trend is nearly buried in the pulse-to-pulse variations.

Above, we gave an argument for tilts and dispersion based on gain guiding and dispersion of the plane-wave phase-matching angle. It is instructive to develop a complementary description based on localized structure in the signal and idler beams that explains the dispersion in terms of temporal and spatial walk-off. For this it is con-

**Table 1. Model Results for a 12-mm-Long Cavity with a 10-mm Crystal and a 6-mJ Pump**

Configuration <sup>a</sup>	<i>e</i> Waves <sup>b</sup>	Resonated Wave <sup>b</sup>	Signal Tilt (mrad)	Shift (GHz)	Bandwidth (GHz)	Dispersion ( $\mu\text{rad}/\text{GHz}$ )
SW	<i>i</i>	<i>i</i>	2.2	360	66	6.1
SW	<i>i</i>	<i>s</i>	3.4	550	133	6.2
SW	<i>s</i>	<i>i</i>	-1.8	310	140	-5.7
SW	<i>s</i>	<i>s</i>	-3.2	570	300	-5.7
SW	<i>p</i>	<i>s</i>	0.16	0	60	
SW	None	<i>s</i>	0	0	40	
SW	<i>s, i</i>	<i>s</i>	-0.5	0	60	
Ring	<i>s</i>	<i>s</i>	0	0	25	
WOC-SW	<i>s</i>	<i>s</i>	0	0	35	

<sup>a</sup>SW, the usual standing-wave OPO but with walk-off and cavity resonance assigned to different beams; ring, single crystal in a three-mirror ring cavity with the same round-trip length; WOC-SW, the usual standing-wave cavity with two walk-off-compensating crystals.

<sup>b</sup>*i*, idler; *s*, signal, *p*, pump.

**Table 2. Signal Tilt for Several Cavity Lengths with a 10-mm Crystal**

Cavity Length (mm)	Measured Signal Tilt (mrad)	Calculated Signal Tilt (mrad)	Measured Pump Threshold (mJ)
12.0	6.6	3.3–3.9	3.1
12.5	6.1		3.35
14.0	5.3		3.4
15.0		2.4–2.6	
16.0	4.7		3.65
17.5	4.4		4.0
20.0	4.0	1.7–2.1	

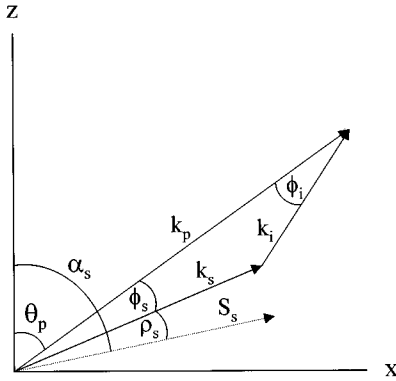


Fig. 6. Noncollinear phase matching for a pump beam propagating at angle  $\theta_p$  relative to the crystal optic axis  $z$ .  $S_s$  is the signal Poynting vector tilted by angle  $\rho_s$  relative to the signal propagation vector  $k_s$ . The Poynting vector makes an angle of  $\alpha_s$  with respect to the optic axis.

venient to express the angular variation of phase-matching angle with signal wavelength in terms of signal and idler group velocities and walk-off angles. We do this by assuming that the contribution to  $\Delta k$  from a small signal tilt cancels that which is due to changes in signal frequency. That is,  $\Delta k_{\text{tilt}} = -\Delta k_{\text{tune}}$  for the noncollinear phase matching shown in Fig. 6. We calculate  $\Delta k_{\text{tilt}}$  for a pump beam propagating at angle  $\theta_p$  relative to optic axis  $z$  and with a small angle between the signal and idler  $k$  vectors. Keeping terms first order in  $d\phi_s$ , we can show straightforwardly that

$$\Delta k_{\text{tilt}} = \frac{2\pi n_s v_s}{c} (\rho_s + \phi_s - \rho_i + \phi_i) \delta\phi_s, \quad (2)$$

where we have used the relation between birefringent walk-off angle  $\rho$  and the refractive index

$$\rho_j = -\frac{1}{n_j} \frac{dn_j}{d\phi} \quad (3)$$

and assumed that

$$\delta\phi_i = \frac{n_s v_s}{n_i v_i} \delta\phi_s. \quad (4)$$

Recalling that the Poynting vector of the signal beam,  $S_s$ , is at angle ( $\alpha_s = \theta_p + \phi_s + \rho_s$ ) and that of the idler is at angle ( $\alpha_i = \theta_p - \phi_i + \rho_i$ ), we rewrite Eq. (2) as

$$\Delta k_{\text{tilt}} = \frac{2\pi n_s v_s}{c} (\alpha_s - \alpha_i) \delta\phi_s. \quad (5)$$

The contribution to  $\Delta k$  from a signal frequency shift of  $\delta\nu_s$  is

$$\Delta k_{\text{tune}} = \frac{2\pi}{c} \left( n_i + \frac{dn_i}{d\nu_i} - n_s - \frac{dn_s}{d\nu_s} \right) \delta\nu_s, \quad (6)$$

assuming that  $\delta\nu_s = -\delta\nu_i$ . Using the definition of group velocity

$$\frac{1}{v_j} = \frac{1}{2\pi} \frac{dk_j}{d\nu_j} = \frac{1}{c} \left( n_j + \nu_j \frac{dn_j}{d\nu_j} \right) \quad (7)$$

yields

$$\Delta k_{\text{tune}} = \frac{2\pi}{c} (g_i - g_s) \delta\nu_s, \quad (8)$$

where we have expressed group velocity  $v_j$  in terms of a group-velocity index  $g_j$  defined by  $v_j = c/g_j$ . The tilt and tune contributions to  $\Delta k$  cancel if

$$\frac{d\nu_s}{d\phi_s} = \frac{n_s v_s (\alpha_s - \alpha_i)}{g_s - g_i}. \quad (9)$$

Outside the crystal this dispersion becomes

$$\frac{d\nu_s}{d\phi_s} = \frac{\nu_s (\alpha_s - \alpha_i)}{g_s - g_i}, \quad (10)$$

assuming small tilts of the exit face. Using the KTP values for group-velocity indices (1.875 and 1.765 for signal and idler, respectively) and walk-off angle (47.5 and 0 mrad for signal and idler, respectively) derived from the same Sellmeier equation,<sup>10</sup> we find the same 3.41- $\mu\text{rad}/\text{GHz}$  internal dispersion as before, corresponding to 6.19  $\mu\text{rad}/\text{GHz}$  external.

This parameterization in terms of group velocity and Poynting vectors suggests an alternative description of dispersion in terms of slanted beam structure. Consider parametric amplification of a short, small-diameter signal pulse by a longer, large-diameter single-mode pump pulse, as depicted at the left in Fig. 7(a). Assuming an undepleted pump, we see that on exiting the crystal the signal and idler beams have the slanted envelopes diagrammed at the right in Fig. 7(a), where slant angle  $\phi$  is given in terms of  $\alpha_j$  and  $g_j$  by

$$\phi = \arctan \left( \frac{g_s - g_i}{\alpha_s - \alpha_i} \right). \quad (11)$$

One could equally well form such slanted pulses by reflecting an unslanted pulse off a diffraction grating, as illustrated in Fig. 7(b). Of course this reflection is associated with angular dispersion, and, from the grating equation, slant  $\phi$  is easily related to grating dispersion  $d\phi/d\nu$  by

$$\phi = \arctan \left( \nu \frac{d\phi}{d\nu} \right), \quad (12)$$

implying by comparison of Eqs. (11) and (12) that the dispersion of the signal and the idler light exiting the crystal can be expressed as

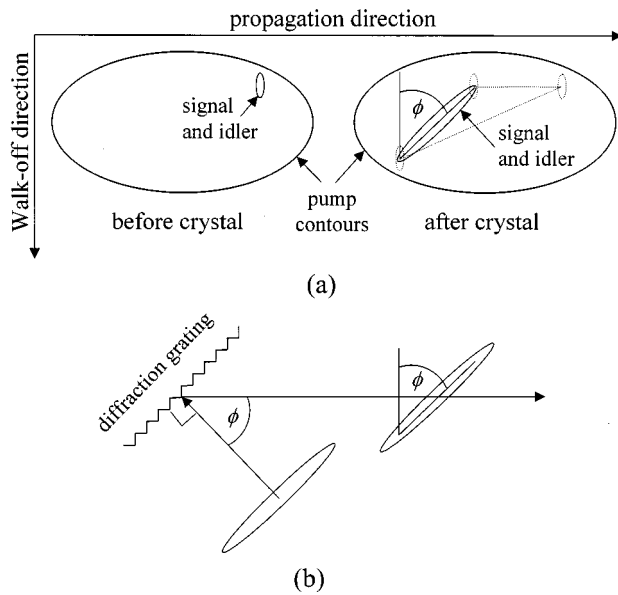


Fig. 7. (a) Parametric amplification of a small-diameter, short-duration signal-idler pulse by a larger, longer pump pulse, illustrating the origin of tilted structure in the amplified signal and idler waves. The ellipses represent half-height contours of irradiance for the input pump, signal, and idler at the left. At the right, the dotted lines show the paths (in the reference frame moving with the pump pulse) that would be followed by the input signal and idler pulses during linear propagation through the crystal. Owing to the combination of group velocity and birefringent walk-off relative to the pump, the input signal and idler pulses trace the lower and upper dotted lines, respectively. The signal and idler light generated in the crystal fills in the slanted ellipse that connects the signal and idler end points. (b) Equivalent slanted pulses can be created by reflection of a short, unslanted signal pulse off a diffraction grating.

$$\frac{dv_s}{d\phi_s} = \frac{v_s(\alpha_s - \alpha_i)}{g_s - g_i}. \quad (13)$$

This equation is identical to Eq. (10), demonstrating the equivalence of descriptions in terms of phase-matched plane waves or slanted envelopes. The latter description is usually invoked in analyzing parametric mixing, for which slanted pulses<sup>11</sup> are used to maintain short pulse durations (implying broad bandwidth), whereas the former is used to describe broad-bandwidth angle-compensated mixing.<sup>12</sup> This implies that, if a mixing process creates slanted structure in the broad-bandwidth signal and idler pulses in an OPO, there will be an angular dispersion given by Eqs. (10) and (13). Such slanted structure is almost inevitable, given spatial and temporal modulation of the signal and idler beams combined with Poynting and group-velocity walk-off. We have verified these effects in detail in a numerical model of single-pass parametric amplification.<sup>13</sup>

It is clear from this understanding of the equivalence of slanted structure and dispersion that the important consideration in eliminating dispersion is that the signal and idler beams have collinear Poynting vectors so there is effectively no lateral walk-off and hence no slanted structure. This is automatically the situation for collinear type I mixing, but for our type II OPO, noncollinear phase matching can accomplish this. If  $k_s$  is assumed to parallel the cavity axis, we can tilt the pump beam slightly to

force  $k_i$ , and thus the idler Poynting vector, to parallel the signal Poynting vector at angle  $\rho_s$ . Doing so requires the pump beam to be tilted in the walk-off direction by

$$\phi_p = \rho_s \frac{n_i \omega_i}{n_p \omega_p} = 15 \text{ mrad}. \quad (14)$$

There will be no slanted structures in this case and hence no dispersion. This is an example of tangential phase matching,<sup>14</sup> the designation for noncollinear phase matching in which the Poynting vectors of an *e* and an *o* wave are parallel. According to Eq. (5), inducing a signal beam tilt by means of a phase mismatch when  $\alpha_s = \alpha_i$  would require a large value of  $\Delta k$ , but then the parametric gain would be severely reduced, so tilts would be suppressed as well as dispersion. We verified this behavior in the laboratory. The OPO behaves much as a type I collinearly phase-matched OPO. The threshold is minimized by tuning of the crystal for zero phase mismatch, and there is no dispersion or tilt. The model produces the same result. This method of eliminating tilts is convenient if the signal-idler tuning range is limited, but for large ranges the pump angle must be adjusted to maintain parallel Poynting vectors. Additionally, the idler will emerge with a large tilt, so the other remedies discussed above may be more attractive in many applications.

Noncollinear pumping of type I OPO's is sometimes used to tune the OPO or to modify the acceptance bandwidth.<sup>15</sup> Because of the association of nonparallel signal and idler Poynting vectors with tilt and dispersion, we expected that these devices would suffer the shortcomings of our standard OPO. Model runs verified this, predicting signal tilt, dispersion, and bandwidths proportional to the angle between the cavity axis and the pump propagation vector.

## 5. INJECTION SEEDING

We have already mentioned that injection seeding was unsuccessful when the crystal was aligned for perfect phase match. In Fig. 5(a) we saw there was no signal light emitted at the seed frequency (zero frequency). However, if we rotate the crystal to shift the signal spectrum to the red (decrease  $\theta$ ) such that its red end coincides with the injected signal frequency, partial seeding is possible, but only if the cavity length is locked to resonate the injected seed light. In Fig. 8 we show the resultant far-field and dispersed images. There is a beam lobe associated with the seed light that has the same frequency as the seed but with a tilt of  $\sim 2$  mrad relative to the seed and cavity axes. We find that to achieve robust seeding it is necessary to tilt the crystal further such that its free-running spectrum is centered on the seed frequency and also to tilt the seed beam so that it is aligned with the median tilt of the free-running OPO. In this case one should be aware of frequency shifts of the order of the cavity's free spectral range as a result both of Fabry-Perot resonance shift with beam tilt and of phase-mismatch-induced frequency shifts.<sup>16</sup> The OPO configurations that eliminate beam tilts, such as the three-mirror ring and the walk-off-compensated standing-wave cavity, seed reliably with no such shifts or tilts.

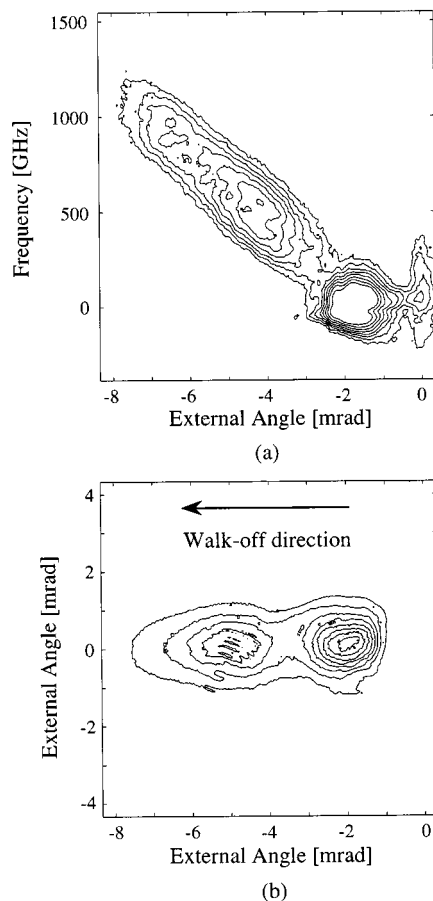


Fig. 8. (a) Measured signal dispersion diagrams showing partial seeding for a crystal tilted to a shift-free running wavelength toward the seed wavelength and (b) the corresponding far-field signal fluence profile.

## 6. CONCLUSIONS

We have shown both in the laboratory and in numerical modeling that standing-wave, nanosecond OPO's with nonparallel signal and idler Poynting vectors generate tilted and dispersed signal and idler beams with large bandwidths. Further, injection seeding these devices requires unusual procedures. These effects can be eliminated by simple modifications of OPO design, including walk-off compensation and image-reversing ring cavities. Because tilt and dispersion are associated with noncollinear signal and idler Poynting vectors, they are inherent in collinear type II OPO's and to noncollinear type I OPO's. However, with proper pump tilts they can be eliminated in noncollinear type II OPO's. We found that injection seeding devices without signal beam tilt is straightforward, with no frequency shifts or tilts of the output light. Cavity mirror misalignment can probably significantly alter the signal tilts and perhaps influence seeding behavior, but it is unlikely to affect the dispersion significantly. We have not systematically studied this issue, but our model could be used to investigate it. Finally, although we did not discuss it, we find that there is relatively little difference in pump threshold or conversion efficiency among the designs covered in this paper.

## ACKNOWLEDGMENTS

This study was supported by the U.S. Department of Energy under contract DE-AC04-94AL85000. Sandia National Laboratories is a multiprogram laboratory operated by Sandia Corporation, a Lockheed Martin Company, for the U.S. Department of Energy.

A. V. Smith's e-mail address is arlsmit@sandia.gov.

## REFERENCES AND NOTES

1. A. V. Smith and M. S. Bowers, "Phase distortions in sum- and difference-frequency mixing in crystals," *J. Opt. Soc. Am. B* **12**, 49–57 (1995).
2. J. G. Haub, R. M. Hentschel, M. J. Johnson, and B. J. Orr, "Controlling the performance of a pulsed optical parametric oscillator: a survey of techniques and spectroscopic applications," *J. Opt. Soc. Am. B* **12**, 2128–2141 (1995).
3. J. G. Haub, M. J. Johnson, A. J. Powell, and B. J. Orr, "Bandwidth characteristics of a pulsed optical parametric oscillator: application to degenerate four-wave mixing spectroscopy," *Opt. Lett.* **20**, 1637–1639 (1995).
4. R. Urschel, U. Bader, A. Borsutzky, and R. Wallenstein, "Spectral properties and conversion efficiency of 355-nm-pumped pulsed optical parametric oscillators of  $\beta$ -barium borate with noncollinear phase matching," *J. Opt. Soc. Am. B* **16**, 565–579 (1999).
5. Y. R. Shen, *The Principles of Nonlinear Optics* (Wiley, New York, 1984).
6. G. Arisholm, "Advanced numerical simulation models for second-order nonlinear interactions," in *Laser Optics '98: Fundamental Problems of Laser Optics*, N. N. Rozanov, ed., Proc. SPIE **3685**, 86–97 (1999).
7. G. Arisholm, "Quantum noise initiation and macroscopic fluctuations in optical parametric oscillators," *J. Opt. Soc. Am. B* **16**, 117–127 (1999).
8. A. V. Smith, W. J. Alford, T. D. Raymond, and M. S. Bowers, "Comparison of a numerical model with measured performance of a seeded, nanosecond KTP optical parametric oscillator," *J. Opt. Soc. Am. B* **12**, 2253–2267 (1995).
9. A. V. Smith, R. J. Gehr, and M. S. Bowers, "Numerical models of broad-bandwidth nanosecond optical parametric oscillators," *J. Opt. Soc. Am. B* **16**, 609–619 (1999).
10. H. Vanherzele, J. D. Bierlein, and F. Zumsteg, "Index of refraction measurements and parametric generation in hydrothermally grown  $\text{KTiOPO}_4$ ," *Appl. Opt.* **27**, 3314–3316 (1988).
11. R. Danielius, A. Piskarskas, P. Di Trapani, A. Andreoni, C. Solcia, and P. Foggi, "A colinearly phase-matched parametric generator/amplifier of visible femtosecond pulses," *IEEE J. Quantum Electron.* **34**, 459–463 (1998).
12. B. A. Richman, S. E. Bisson, R. Trebino, E. Sidick, and A. Jacobson, "Efficient broadband second-harmonic generation by dispersive achromatic nonlinear conversion using only prisms," *Opt. Lett.* **23**, 497–499 (1998).
13. This case was modeled with function 2Dmix-SP in the SNLO software package, which is freely distributed at <http://www.sandia.gov/imrl/XWEB1128/xxtal.htm>.
14. M. J. T. Milton, T. J. McIlveen, D. C. Hanna, and P. T. Woods, "High-efficiency infrared generation by difference-frequency mixing using tangential phase matching," *Opt. Commun.* **87**, 273–277 (1992).
15. G. C. Bhar, U. Chatterjee, and S. Das, "Tunable near-infrared radiation by difference frequency mixing in beta barium borate crystal," *Appl. Phys. Lett.* **58**, 231–233 (1991).
16. T. D. Raymond, W. J. Alford, A. V. Smith, and M. S. Bowers, "Frequency shifts in injection-seeded optical parametric oscillators with phase mismatch," *Opt. Lett.* **19**, 1520–1522 (1994).